SLAC-PUB-2425
November 1979
(T/E)

RESULTS FROM THE CRYSTAL BALL DETECTOR AT SPEAR*

Crystal Ball Collaboration[1]

Presented by Elliott D. Bloom
Stanford Linear Accelerator Center
Stanford University, Stanford, California 94305

Introduction

The Crystal Ball detector is a device particularly suited to the measurement of photons with energies lower than 1 GeV. As shown in Fig. 1, the detector has as its principal component a 16 radiation length thick highly segmented shell of NaI(Tℓ) surrounding cylindrical proportional and magnetostrictive spark chambers. The main Ball and various elements of the central chambers cover 94% of 4π sr. Segmented endcap NaI(Tℓ) detectors of 20 radiation lengths behind magnetostrictive spark chambers supplement the main Ball. The Ball and endcaps close the solid angle for charged particle and photon detection to 98% of 4π sr. In addition (not shown in Fig. 1), detectors of interspersed iron and proportional tubes provide for μ-π separation over 15% of 4π sr. about $\theta_{CM} = 90^{o}$. A more complete description of the detector, its electronics, calibration and triggers can be found in Ref. 2.

The Crystal Ball collaboration[1] has concentrated on two projects since SPEAR data taking begin in December 1978:

(1) A detailed study of the charmonium system. Data taking has been completed. Approximately 900K events at the J/ψ, 800K events at the ψ' and 50K events at ψ'' have been obtained.

(2) A study of R_{hadron}, neutral energy, multiplicities, and other inclusive characteristics of the continuum above 3.9 GeV. This has been started and a fine energy scan has been made from $E_{CM} \sim 3.9$ GeV to $E_{CM} \sim 4.5$ GeV. In addition extensive data were obtained at $E_{CM} = 5.2$ GeV and 6.5 GeV.

In this report preliminary results will be presented from the data obtained as described in (1) and (2) above. In particular, QED at $E_{CM} = 6.5$ GeV, R_{hadron} and related inclusive distributions, η branching fractions at J/ψ and ψ'', and a detailed study of the psionium system will be discussed.

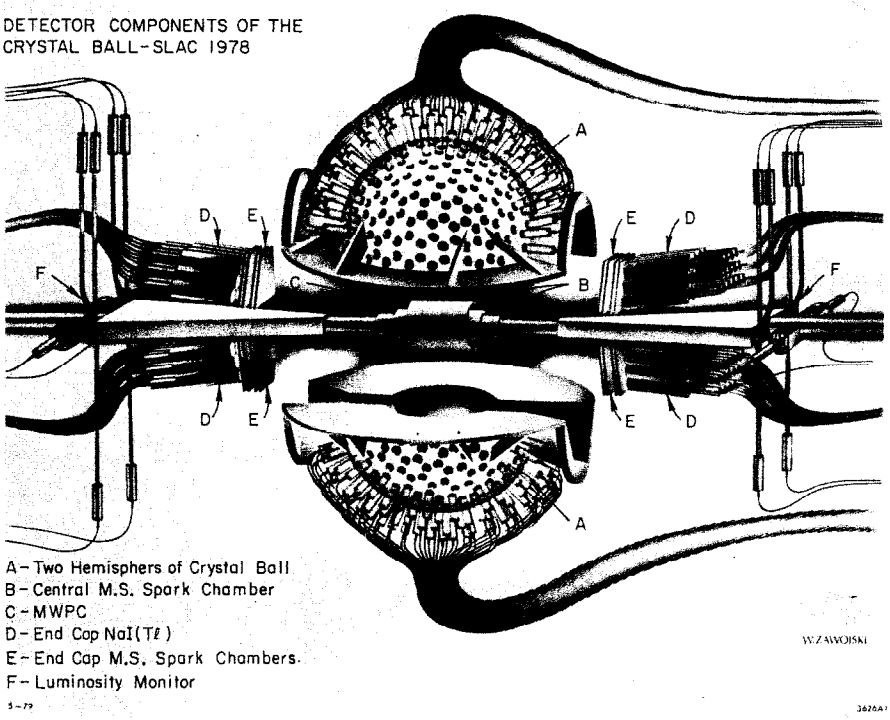

Fig. 1. An artist's rendition of the major components of the crystal detector system. The main Ball of 672 segments of NaI(Tℓ) covers 94% of 4π sr. The central tracking chambers are in three layers. The first layer is 2 gaps of magnetostrictive spark chambers covering 94% of 4π sr. The next layer is a double gap multiwire proportional chamber covering 80% of 4π sr. The final layer is 2 more gaps of magnetostrictive spark chamber covering 70% of 4π sr. The endcap NaI(Tℓ) and 4 gaps of magnetrostrictive spark chambers close the solid angle to 98% of 4π sr.

* Work supported in part by the Department of Energy under contract numbers DE-AC03-76SF00515 (SLAC), DE-AC03-79ER0068 (Caltech), and EY-76-C-02-3064 (Harvard); and by the National Science Foundations numbers PHY 78-00967 (HEPL) and PHY 78-07343 (Princeton).

(Invited talk presented at the 1979 International Symposium on Lepton and Photon Interaction at High Energy, Batavia, Illinois, August 23-29, 1979.)

QED and Tests of the Apparatus

One of the simplest physics processes to observe in the Ball is the QED reaction,

$$e^+e^- \rightarrow \gamma\gamma \qquad (1)$$

The cuts used to select events for this process are shown in Table I.

Table I

Selection Criterion for Events
Contributing to $e^+e^- \rightarrow \gamma\gamma$

(1)	More than one major contiguous region of energy deposition (connected energy region) in the Ball.
(2)	Two to four neutral particles identified by pattern recognition. (2 to 4 energy bumps with no associated chamber hits.)
(3)	Two neutral particles with $E \geq 0.7\ E_{beam}$.
(4)	$\lvert\cos\theta_\gamma\rvert \leq 0.85$, where θ_γ is the photon angle to the e^+ beam.

A typical event, obtained at $E_{CM} = 7.4$ GeV, is shown in Fig. 2. As seen in the figure, the photons have a lateral energy spread in the Ball, with a number of modules having appreciable energy deposition. Typically for identified photons, the 12 modules around the module with the largest energy deposition, and this module are summed for analysis. Approximately, 95% of the energy of the photon is contained in this sum of 13 modules. Correction for average energy loss is easily made. The lateral shower spread is used to determine the direction of photons more accurately than a single module size would allow. For example with $E_\gamma \sim 1.5$ GeV we presently obtain $\sigma_{\theta projected} \sim 1^o$. A single Ball module is $\approx 12^o$ on a side and geometrically yields $\sigma_{\theta projected} \approx 3.5^o$. The angular resolution worsens as E_γ lowers, with $\sigma_{\theta projected} \sim 2.5^o$ presently obtained at $E_\gamma \sim 100$ MeV.

The resulting events are corrected for radiative effects (0.975), and γ conversion in the beam pipe and tracking chambers (.94). After dividing by the luminosity, known to ±3% from an independent luminosity monitor (see Fig. 1), an absolute cross section is obtained. Figure 3 shows the absolute differential cross section measured at $E_{CM} = 6.5$ GeV, divided by QED theory. Good agreement to $\lesssim \pm 10\%$ is found over the entire angular range displayed. A point-to-point

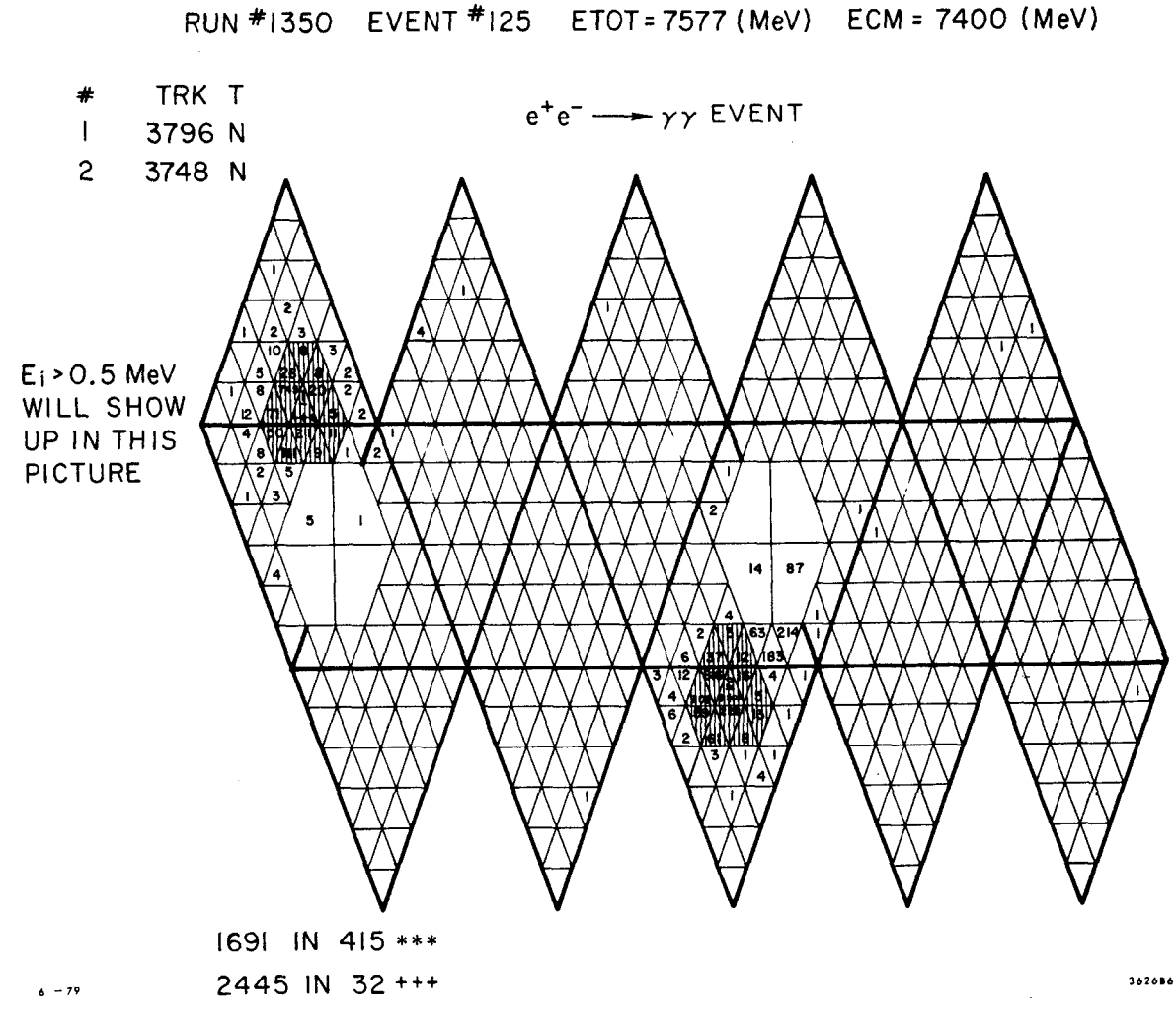

Fig. 2. A typical $e^+e^- \rightarrow \gamma\gamma$ event at $E_{CM} = 7.4$ GeV. Each of the 672 modules of the Ball is represented as a small triangle; the endcap quadrants are shown without segmentation (each quadrant subtends 1% of 4π sr). The major triangles (bold outline) correspond to the underlying faces of the icosahedron which define the basic geometry of the Ball. Each module, i, with an energy deposition of $E_i \geq 0.5$ MeV shows an integer 1-999 (> 999 = xxx) representing the energy measured in MeV. This is also true for each endcap quadrant. The sum of 13 modules yielding the energy and angle measurement for each photon is shown by the cross lined regions.

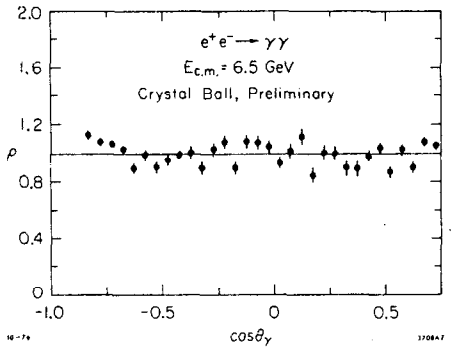

Fig. 3. $\rho(\cos\theta_\gamma) = \sigma_{exp}(\cos\theta_\gamma)/\sigma_{QED}(\cos\theta_\gamma)$ for $|\cos\theta_\gamma| \leq 0.80$. 60% of the data obtained at E_{CM} = 6.5 GeV is shown. The errors shown are statistical only. An additional systematic error of ±10% is estimated; much of this error is thought to be point-to-point and may be due to the systematics of our current angle finding algorithms.

deviation is seen, however, which exceeds statistical expectations. Figure 4 shows the ϕ_γ distribution for $\gamma\gamma$ events at E_{CM} = 1.842 GeV. Again the expected uniform ϕ_γ dependence is obtained to the ±10% level. A non-random deviation seen in this distribution is somewhat correlated with the boundary between the two hemispheres of the Ball. Comparisons between Monte Carlo generated events and real physics events have indicated the existence of some bias in our present angle finding algorithms. Basically, these algorithms have a bias toward the center of a module. The particular geometry of the Ball then makes projections of θ_γ and ϕ_γ "bumpier" than ideally expected. We estimate that these small biases have only a minor effect on the physics results presented in this report.

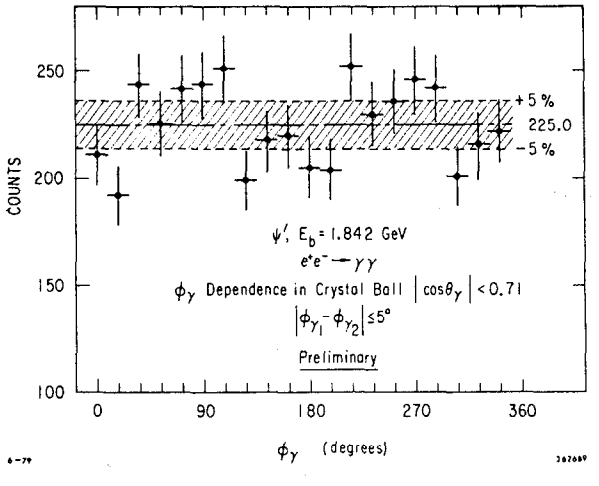

Fig. 4. The number of counts/(10^o $\Delta\phi_\gamma$) vs. ϕ_γ, E_{CM} = 3.684 GeV (ψ'), and $|\cos\theta_\gamma| <$ 0.71. Note the suppressed zero. Again point-to-point systematics of as much as ±10% are seen. These non-statistical fluctuations tend to correlate with the boundaries of the two hemispheres of the Ball at 0^o and 180^o. We expect that current angle finding algorithms are producing the discontinuities as they do not compensate for the differing shower behavior near the hemispheres boundaries.

On integrating over $\cos\theta_\gamma$, excellent agreement is obtained with QED as shown in Fig. 5. The error bars for Crystall Ball results are mainly systematic error estimates. The results of previous experiments are also shown.[3-8]

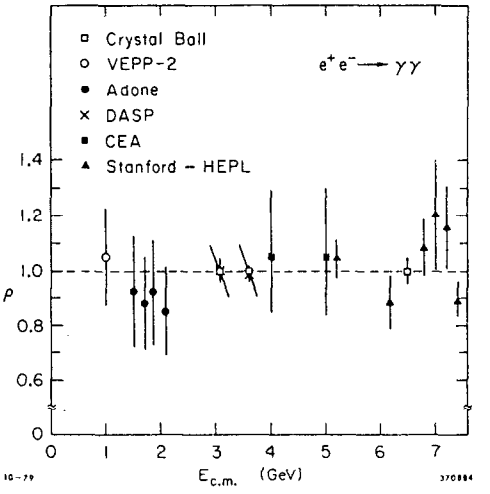

Fig. 5. ρ vs. E_{CM} for various experiments. Crystal Ball values are obtained by integrating over the angular range, $|\cos\theta_\gamma| < 0.71$, for $E_{CM} = M_\psi$ and $M_{\psi'}$; an integral over the angular distribution of Fig. 3 was made to obtain the point at E_{CM} = 6.5. Essentially all the contribution to the errors on the Crystal Ball points are estimates of systematic effects.

Measurement of R_{hadron}, Multiplicities and Neutral Energy

(a) The Selection of Hadronic Events and R_{hadron}

Figure 6(a) shows the measured total energy distribution for all events allowed by the Crystal Ball triggers at E_{CM} = 4.0 GeV; also shown as the dotted line is the extracted multi-hadron signal. Clearly there is a large background. Even though in this energy region the total calorimetry of the Ball is good ($\sigma_{E_{meas}} \sim 25\%$), calorimetry alone is not sufficient to separate the hadronic signal from cosmic ray, beam gas, QED, and other backgrounds.

In order to separate the multi-hadronic component of the triggers, a number of cuts are needed, these are shown in Table II. The resulting measured total energy distribution for multi-hadronic events (including some $\bar{\tau}\tau$ events) is shown in Fig. 6(b).

Figure 7 shows the measured Z distribution of events satisfying cuts 1-6 of Table II. The additional Z cut requirement of $|Z| < 12$ cm ($\sigma^Z_{beam} \sim 2$-3 cm) has only a small effect on the resulting cross section.

After dividing by the integrated luminosity obtained from our independent small angle luminosity monitor, correcting for the multihadron efficiency resulting from the cuts of Table II, radiatively correcting, and subtracting the remnant $\tau\bar{\tau}$ contribution (~ 0.4 unit of R), we obtain preliminary values of R_{hadron} as shown in Fig. 8. In the figure only the statistical errors are shown; additional systematic errors of ±12% are estimated. The largest contribution to the systematic error is the uncertainty in the multihadron efficiency (91% ± 7%).

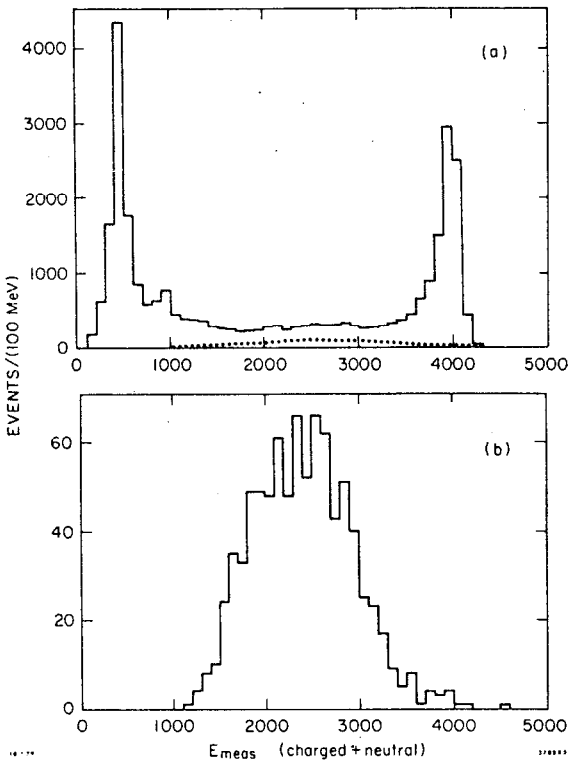

Fig. 6. (a) $E_{measured}$ (charge + neutral) vs. counts/100 MeV for all events allowed by the Crystal Ball triggers at E_{CM} = 4.0 GeV. The dotted line is the extracted multihadron signal also shown on a different vertical scale in Fig. 6(b). (b) $E_{measured}$ (charged + neutral) vs. counts/100 MeV for events satisfying the cuts of Table II. These events are essentially multihadrons plus some $\tau\bar{\tau}$ events.

Table II

Selection Criterion for
Multihadron Events (off resonance)

(1) $E_{TOT} \geq 0.46 * E_{beam}$.

(2) $E(|\cos\theta_i| < 0.85)/E_{TOT} > 0.5$, θ_i is the particle angle to the e^+ beam.

(3) > three connected energy regions with E_{region} > 50 MeV.

(4) ≥ three (neutral + charged) tracks with E_{track} > 20 MeV.

(5) At least one reconstructed charged particle track, which defines a vertex.

(6) $|\Sigma\vec{P}_i|/\Sigma|\vec{P}_i| < 0.65$, where the sums are over all particles in the event, and $\vec{P}_i$ is the measured momentum assuming each charged particle is a pion, and each neutral particle is a photon (NaI(Tℓ) measures deposited energy).

(7) $|Z_{vertex}| < 12$ cm (see Fig. 7).

(8) Beam gas and cosmic ray remnants are subtracted statistically run by run, using separated beam measurements.

Note: We estimate the total efficiency for multihadrons to be 91% ± 7% based upon simple Monte Carlo studies.

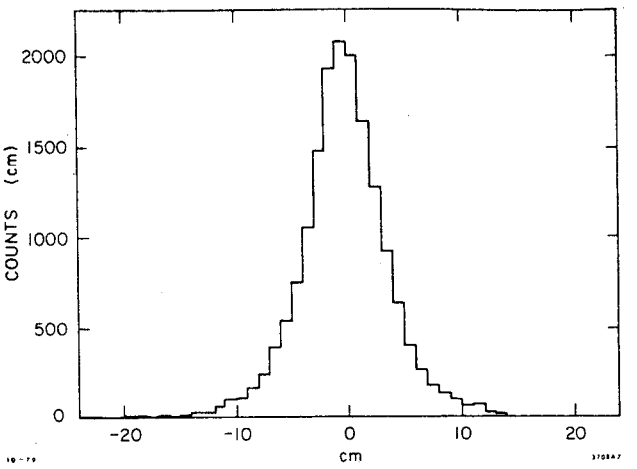

Fig. 7. Z(cm) vs. counts/cm for events obtained by cuts 1-6 of Table II. The background to beam, beam interaction associated events is small.

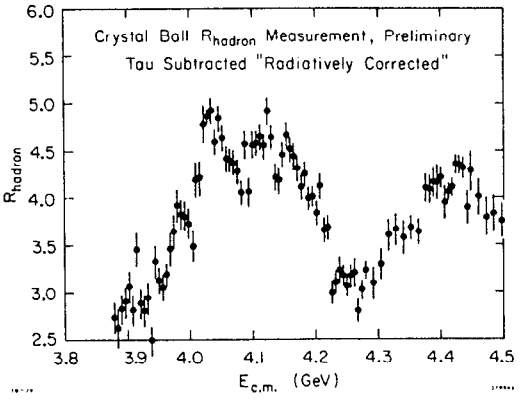

Fig. 8. R_{hadron} vs. E_{CM} from the Crystal Ball. The measurement is preliminary. Only statistical errors are shown in the figure, and additional systematic error of ±12% is estimated. Note that the values of R shown have $R_{\tau\bar{\tau}}$ subtracted.

The major features of R_{hadron} seen in Fig. 8 are similar to those seen in previous measurements of R[9-10].

We have also measured R at 5.2 GeV with good statistical precision (not shown in Fig. 8). After treating this data as we did the 4 GeV region data, we obtain the preliminary result,

$$R_{hadron} = 3.8 \pm 0.1 \pm 0.5 \ , \quad E_{CM} = 5.2 \text{ GeV} \ . \qquad (2)$$

The statistical error is shown first, our estimate of systematic error is shown separately last. This result is in good agreement with a DELCO Measurement[10] (also $\tau\bar{\tau}$ subtracted) at E_{CM} = 5.1 GeV.

(b) Multiplicities and Neutral Energy Fraction

Using the events of our multihadron sample with the additional requirements that E_{track} > 40 MeV (this requirement implies, $P_{\pi^\pm} \gtrsim 100$ MeV), and cos $\theta_{\gamma\text{-charged}}$ < 0.925, we obtain preliminary multiplicities as shown in Fig. 9. Note that these multiplicities are corrected for acceptance, but not corrected for γ conversion,

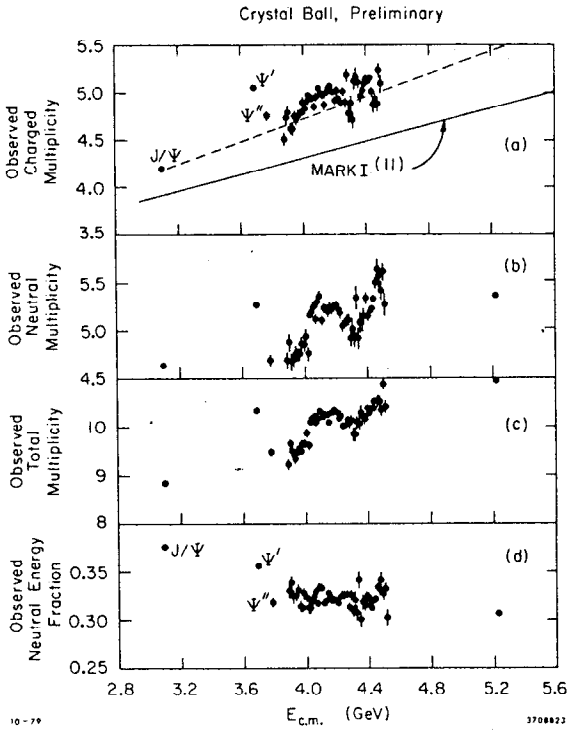

Fig. 9. Inclusive distribution for hadrons for J/ψ, ψ', ψ'', and 4 GeV continuum region. All distributions are corrected for acceptance, but not for other effects (see text). (a) Observed charged multiplicity; (b) observed neutral multiplicity; (c) observed total multiplicity, and (d) observed neutral energy fraction essentially ΣE_γ (> 40 MeV)/E_{CM}.

tracking inefficiency, or $\tau\bar{\tau}$ contributions. The errors shown in Figs. 9(a)-(d) are statistical only. Figure 9(a) shows our preliminary measurement of the charge multiplicity as a function of E_{CM}. The solid line is a fit to Mark I data[11] of the form,

$$\langle N_c \rangle = a + b\, \ell n(E_{CM}) \qquad (3)$$

The dotted line is an eyeball linear fit to Crystal Ball data. On the average our data is 0.5 unit higher than the Mark I fit, however, γ-conversions contribute approximately 0.2 units of multiplicity to our result. More supprising, our data shows obvious structure which deviates significantly from a fit of the form of Eq. (3).

Even more structure is seen in the preliminary neutral multiplicity vs. E_{CM} in Fig. 9(b). Note that $E_\gamma \gtrsim 40$ MeV, $p_{\pi^o} \gtrsim 0.0$ for tracks contributing to the neutral multiplicity. One expects extra, low energy π^o's and γ's from $D^* \to \pi^o D$, γD transitions at various E_{CM} in this energy range, e.g., at $E_{CM} = 4.03$ GeV[12] where $E_{\pi o} \sim E_\gamma \sim 145$ MeV. Also processes such as $F^* \to \gamma F$ may be contributing to the observed structure.

Figure 9(c) shows preliminary values of the total particle multiplicity vs. E_{CM}. The amount of structure seen in the total multiplicity is somewhat subdued as compared to that of neutral multiplicity.

Figure 9(d) shows the observed neutral energy fraction, $E_{neutral}/E_{CM}$ vs. E_{CM}. This quantity has a rather large value at the J/ψ, but in the continuum region it assumes the prosaic value of ~1/3. As E_{CM} increases, $E_{neutral}/E_{CM}$ may drop slightly.

In Crystal Ball measurements the main component of $E_{neutral}$ which is directly observed are photons with $E_\gamma > 40$ MeV. In previous Mark I measurements[11] $E_{CM} - E_{charged}$ was used to infer $E_{neutral}$. The preliminary Crystal Ball results shown in Fig. 9(d) thus indicate that the previously observed rise with E_{CM} of $(E_{CM} - E_{charged})/E_{CM}$, the "energy crisis", is not due to photons with $E_\gamma \gtrsim 40$ MeV.

Inclusive η Branching Fraction at J/ψ and ψ''

Figure 10 shows a distribution of the mass of all photon pairs with $M_{\gamma\gamma} > 300$ MeV. The data shown were obtained at $E_{CM} = 3.772$ GeV (ψ''). A signal at the η mass is evident. No cuts other than hadronic cuts similar to those of Table II have been applied to the events. A similar distribution was produced for J/ψ data. Both distributions were fit to a Gaussian centered at a fixed mass of the η with fixed experimental mass resolution, plus a variable polynominal background. The η mass, M_η, and resolution, σ_M, were found from a fit to data at the J/ψ with good statistics to be,

$$M_\eta = 543 \pm 11 \text{ MeV} \quad , \quad \sigma_M = 22 \text{ MeV} \quad , \qquad (4)$$

where the error on M_η is mainly systematic. After radiative corrections the preliminary results for the inclusive branching fraction are,

$$\begin{aligned} Br(J/\psi \to \eta + x) &= 0.12 \pm 0.03 \pm 0.04 \\ B(\psi'' + \text{continuum} \to \eta + x) &= 0.19 \pm 0.03 \pm 0.06 \ . \end{aligned} \qquad (5)$$

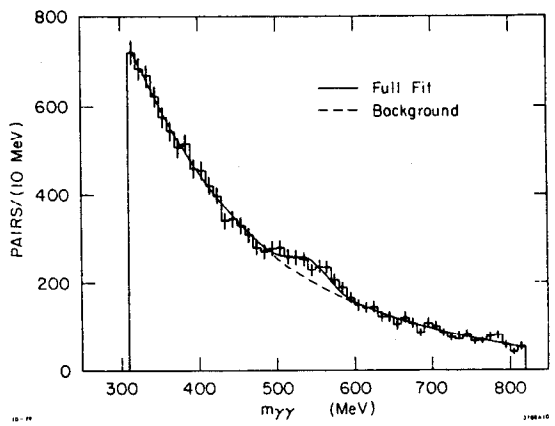

Fig. 10. $M_{\gamma\gamma}$ distribution from ψ'' for $M_{\gamma\gamma} > \sim 300$ MeV. An $\eta(548)$ signal is evident.

The first error is the statistical error estimate of the fit. The second error is our estimate of systematic effects - primarily acceptance. We expect that some of the second systematic error would cancel in a ratio between the two numbers.

The result (5) is considerably smaller for the J/ψ than the $\gtrsim 0.4$ previously estimated.[13] This unexpectedly low η inclusive branching fraction when combined with the large neutral energy fraction at J/ψ and the analysis of Ref. 13, implies a still undetermined source of photons in J/ψ decays. A candidate for such a source are the prompt γ's predicted by QCD[14] in γgg decay of the J/ψ.

The Psionium System

Figure 11 shows the states of psionium, interpreted by the charmonium model, at the time of the last lepton-photon conference.[15] Since that time, and particularly as Crystal Ball measurements have become available over the past 6 months, the picture has radically changed. At the time of the Hamburg Conference the η_c' candidate $\chi(3455)$ had been seen by 3 experiments and published by one.[3,16] The second photon in the $\chi(3410)$ cascade also seemed well established at a rate consistent with QCD predictions.[17]

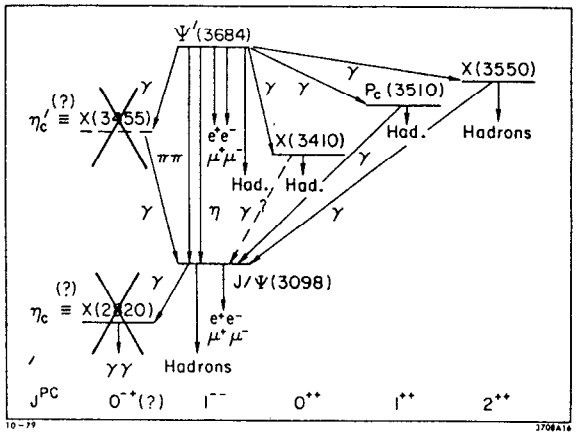

Fig. 11. The state of knowledge of the psionium system, as interpreted by the charmonium model, at the last lepton photon conference (minus crosses). The crosses are some of the contributions of the Crystal Ball herein reported.

The η_c candidate X(2820) had been seen in one experiment,[18] while another experiment[19] using hadron beams provided weaker supporting evidence for a meson in that mass range (2.8-3.0 GeV). The existence of the intermediate states X(3550), P_c/X(3510), X(3410) was firmly established from measurements of inclusive photon spectra[20,21] as well as cascade decays of the ψ'.[3,16] However, that these states were the intermediate P-states sought in non-relativistic charmonium models[22] was based more on theoretical prejudice than experimental fact.[16,17] Indeed, given the difficulty the theoretical models had with X(3455) and X(2820) being the 0^{-+} states of charmonium, little hard experimental evidence existed which supported the details of the popular models.[23,24] On examining the totality of experimental evidence then available, a natural conclusion was that the non-relativistic charmonium model of the J/ψ, ψ' system was basically flawed. The existence of the X(2820) and X(3455) thus became pivotal elements in the theoretical understanding of the psionium system. The crosses in Fig. 11 anticipate the results from the Crystal Ball presented in Sections (a) and (b). It appears the theorists may breath a sigh of relief.

(a) J/ψ → 3γ and the Existence of X(2820)

Figure 12 shows the extent of our data taking at the J/ψ and ψ'. The units of the figure are $\mathscr{L}(nb^{-1})$. The total number of J/ψ's obtained was approximately 900K, the total number of ψ's was approximately 800K. All of these data have now been analyzed for the processes

$$J/\psi \rightarrow 3\gamma \qquad (6)$$

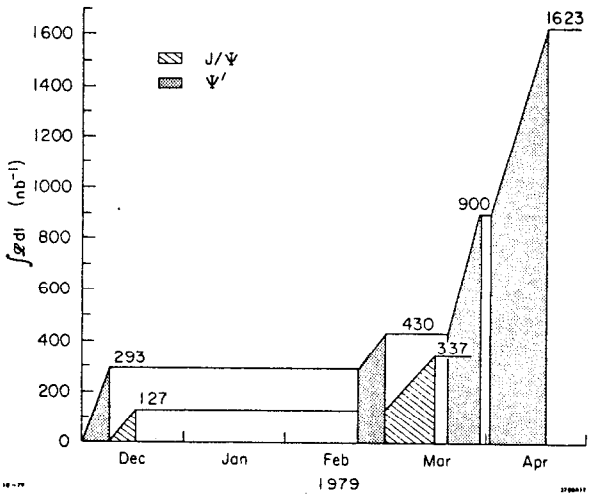

Fig. 12. J/ψ and ψ' data taking of the Crystal Ball for December 1978 through April 1979. Approximately 800K ψ' and 900K J/ψ were obtained.

$$\psi' \rightarrow \pi^+\pi^- J/\psi \quad (\rightarrow 3\gamma) \qquad (7)$$

Processes (6) and (7) bare directly on the question of the existence of the DASP X(2820). We have discussed process (6) previously,[2,25] thus I will only quickly review our result here. Figure 13 shows events of process (6) obtained from our entire J/ψ data sample. The Dalitz plot is shown, and the dotted line indicates the expected location of X(2820). We expect a clustering of $\gtrsim 50$ events about this line if the DASP branching fraction is used. No such clustering is observed, and a fit to the Dalitz plot yields,

$$Br(J/\psi \rightarrow \gamma X(2820)) \times (X \rightarrow \gamma\gamma) < 0.3 \times 10^{-4} \quad (90\%\ C.L.) \qquad (8)$$

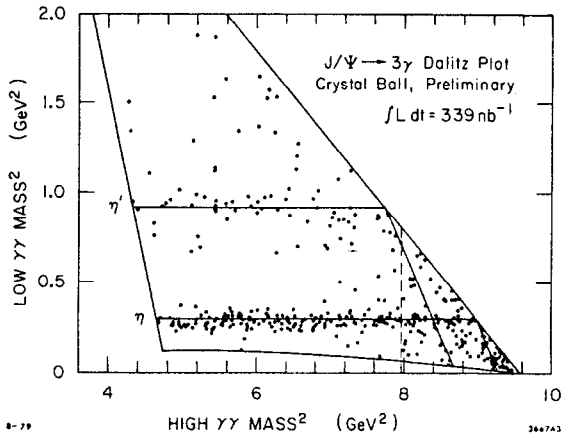

Fig. 13. The J/ψ → 3γ Dalitz plot, the η and η' signals are clearly evident as is a general background arising from the QED 3γ process. The vertical dashed line indicates the expected position of the DASP X(2820); $\gtrsim 50$ events are expected clustering about this line.

As an independent check to the upper limit (8), we have considered the process (7). In considering (7) the 3γ QED background present in (6) arising from

radiative corrections to process (1), will be totally absent. Thus a much cleaner Dalitz plot will result.

A typical event of process (7) is shown in Fig. 14. The selection criteria for these events are given in Table III.

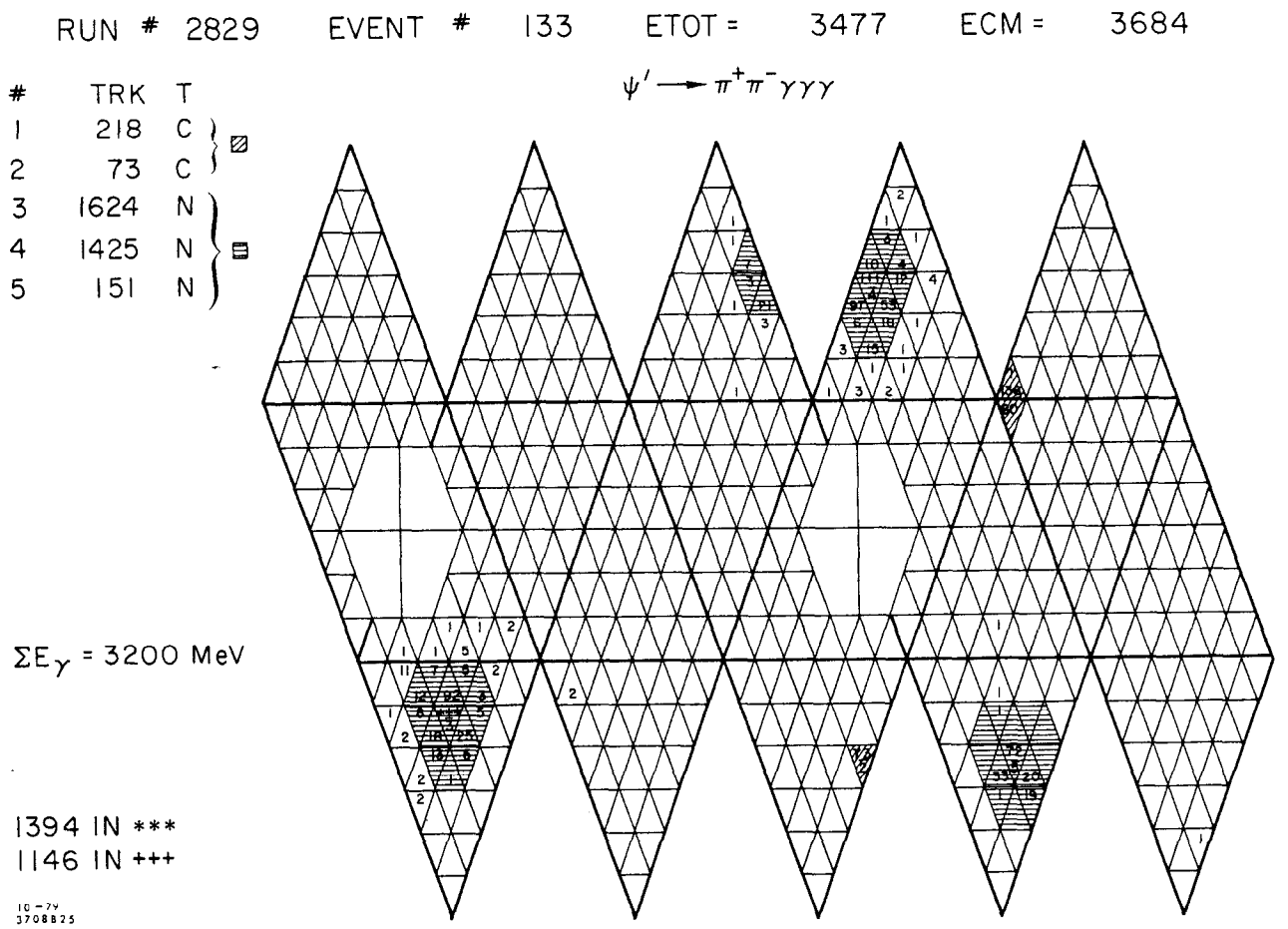

Fig. 14. A typical event of process (7). The sum of 13 modules is shown for photons, while for identified charged particles smaller numbers of crystals are summed. In the legend in the upper left, charged particles are denoted by C, photons by N. The energy of the particles as measured in the Ball is given under TRK.

Table III

Selection Criteria for Events of Process (7)

(1) All particles have $|\cos\theta_i| < 0.9$, θ_i is the particle angle to the e^+ beam.

(2) Two charged particles plus 3 neutrals in the event.

(3) $E_\gamma > 20$ MeV.

(4) Angle between pairs of particles, $\cos\theta_{ij} < 0.9$.

(5) $8\ \text{GeV}^2 \leq M^2_{neut} \leq 11\ \text{GeV}^2$.

(6) 3C fit satisfied with $\chi^2 < 30$.

The resulting preliminary Dalitz plot is shown in Fig. 15. Essentially only $\gamma\eta$ and $\gamma\eta'$ decays are seen. The dotted lines indicate the range of M^2_{high} in which X(2820) events should appear given our estimated resolution. No events are seen in this band which are outside the $\gamma\eta$ band. Using the ratio of our measured $\gamma\eta$ and $\gamma\eta'$ yield for this process to the yields from process (6), and independent Monte Carlo estimates of efficiency we find preliminary values,

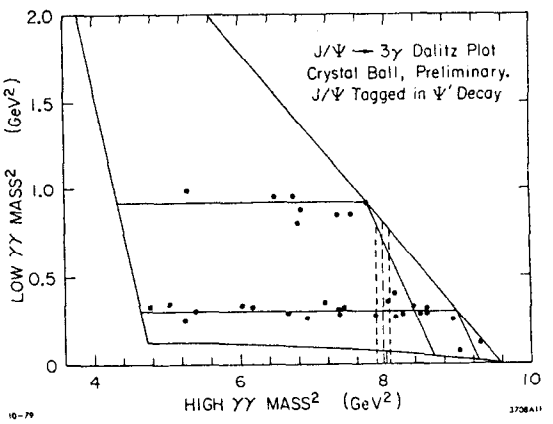

Fig. 15. Dalitz plot for $J/\psi \rightarrow 3\gamma$ resulting from the analysis of process (7). The η and η' signals are clearly seen, no other signal is evident. In particular, the vertical dashed lines indicate the 1σ limits of the expected X(2820) band. Approximately 6 X(2820) events are expected outside the 2σ limits of the η band, at most 1 event is observed.

$$Br(J/\psi \to \gamma X(2820)) < .5 \times 10^{-4} \text{ (90\% C.L.)}$$
$$\hookrightarrow \gamma\gamma \quad , \qquad (9)$$

and, including one event which lies closer to the X band than any other band we obtain,

$$Br(J/\psi \to \gamma X(2820)) < .8 \times 10^{-4}$$
$$\hookrightarrow \gamma\gamma \qquad (10)$$

We also find,

$$Br(J/\psi \to \gamma\eta'/J/\psi \to \gamma\eta) = 7.9 \pm 3.6 \qquad (11)$$

These values compare well with our previously reported values[2,25] obtained from process (6).

A summary of DASP and Crystal Ball results is shown in Fig. 16. The upper limits shown are for a narrow η_c, that is one narrower than the present Crystal Ball resolution (~8.5 MeV FWHM @ E_γ = 100 MeV). The theory is from Ref. 22. The figure indicates that after examining the two processes (6) and (7) the Crystal Ball has no signal for the DASP X(2820).

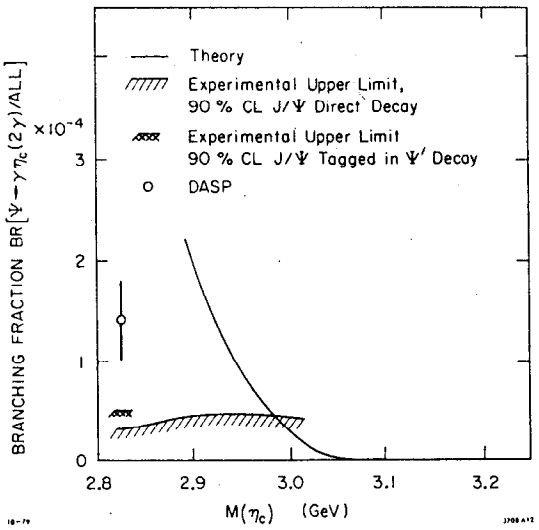

Fig. 16. Summary of results for $J/\psi \to 3\gamma$ using processes (6) and (7). The theory is that of Ref. 22. Note that the upper limit shown for process (7) assumes no X(2820) candidates seen. Including the one possible candidate closer to the X band than η or η' bands raises the limit to 0.8×10^{-4}.

(b) The ψ' Gamma Cascades and the Existence of $\chi(3455)$

All of our ψ' events have been analyzed for the ψ' gamma cascade process,

$$\psi' \to \gamma\chi$$
$$\hookrightarrow \gamma\ J/\psi$$
$$\hookrightarrow \ell^+\ell^- \qquad (12)$$

A typical example of which is shown in Fig. 17. This analysis yields a total of 1705 candidates after the cuts described in Table IV are applied.

Table IV

Selection Criteria for Events of Process (12)

(1)	$E_{TOT} = \begin{cases} 3.3 \text{ GeV to } 4.3 \text{ GeV for } e^+e^-\gamma\gamma \\ 0.97 \text{ GeV to } 1.3 \text{ GeV for } \mu^+\mu^-\gamma\gamma \end{cases}$.
(2)	Energy in endcaps < 5 MeV. (Helps remove $\pi^o\pi^o$ background.)
(3)	Two charged particles; 2 neutral particles with $E_{neut} \geq 40$ MeV.
(4)	$\lvert\cos\theta\rvert < 0.9$ for all particles, θ_i is the particle angle to the e^+ beam.
(5)	Angle between pairs of particles, $\cos\theta_{ij} < 0.9$.
(6)	490 MeV < $(E_{\gamma_1} + E_{\gamma_2})$ < 660 MeV.
(7)	3C fit for $\mu^+\mu^-\gamma\gamma$, 5C fit for $e^+e^-\gamma\gamma$.
(8)	$M_{\gamma\gamma} < 530$ MeV (remove η).

The sequence of cuts of Table IV is partially demonstrated in Fig. 18. Figure 18(a) shows the data after cuts 1-5 of Table IV have been applied. The data is plotted High Mass $(\gamma - J/\psi)$ vs. Low Mass $(\gamma - J/\psi)$. Note that the masses are derived from direct photon energy measurement. The "raw data" (unfit) of Fig. 18(a) clearly shows X(3555) and X(3510) signals. An η signal is also visible as a band of events on the upper left, sloping downward to the right. After fitting (step (7) of Table IV), the data appears as shown in Fig. 18(b)). The requirements of energy-momentum conservation and J/ψ mass for the lepton-pair mass, impose the kinematic limits evident in Fig. 18(b). The observed X states are seen as vertical bands in the figure; the η having a specific $\gamma\gamma$ mass has been compressed to a stripe sloping downward to the right from the upper left. The kinematic fit dramatically improves the η mass resolution, and as seen in Fig. 19 results in an η mass resolution of ~2.7% FWHM. Using Fig. 19, as a guide, step (8) of Table IV seems reasonable. After rejecting the η's by a simple mass cut, the data appear as in Fig. 18(c), or projected vs. High Mass as in Fig. 20. As is seen in Fig. 20, two X state signals are quite evident, with no other signal being seen. We have extracted branching fractions and upper limits from the data of Fig. 20 by applying Monte Carlo calculations of our efficiency (typically ~50%), dividing by our measured ψ' yield and subtracting Monte Carlo estimates of $\pi^o\pi^o$ background. These numbers along with their estimated systematic errors appear in Table V.

The Crystal Ball results of Figs. 18 and 20, and Table V appear in strong contrast to many of the results of previous experiments shown in Fig. 21 and Table VI. In particular the claimed existence of the states X(3455)[28] and X(3591) are not confirmed by our data. Also our limit on the X(3410) cascade, process (12) is much smaller than previous results. Note that the existence of the X(3410) is not being challenged, because a strong signal at that mass is seen in the inclusive γ spectrum from the ψ' (cf. Section (e)). However, the small branching fraction for the second photon in the cascade has interesting implications for QCD as I will discuss.

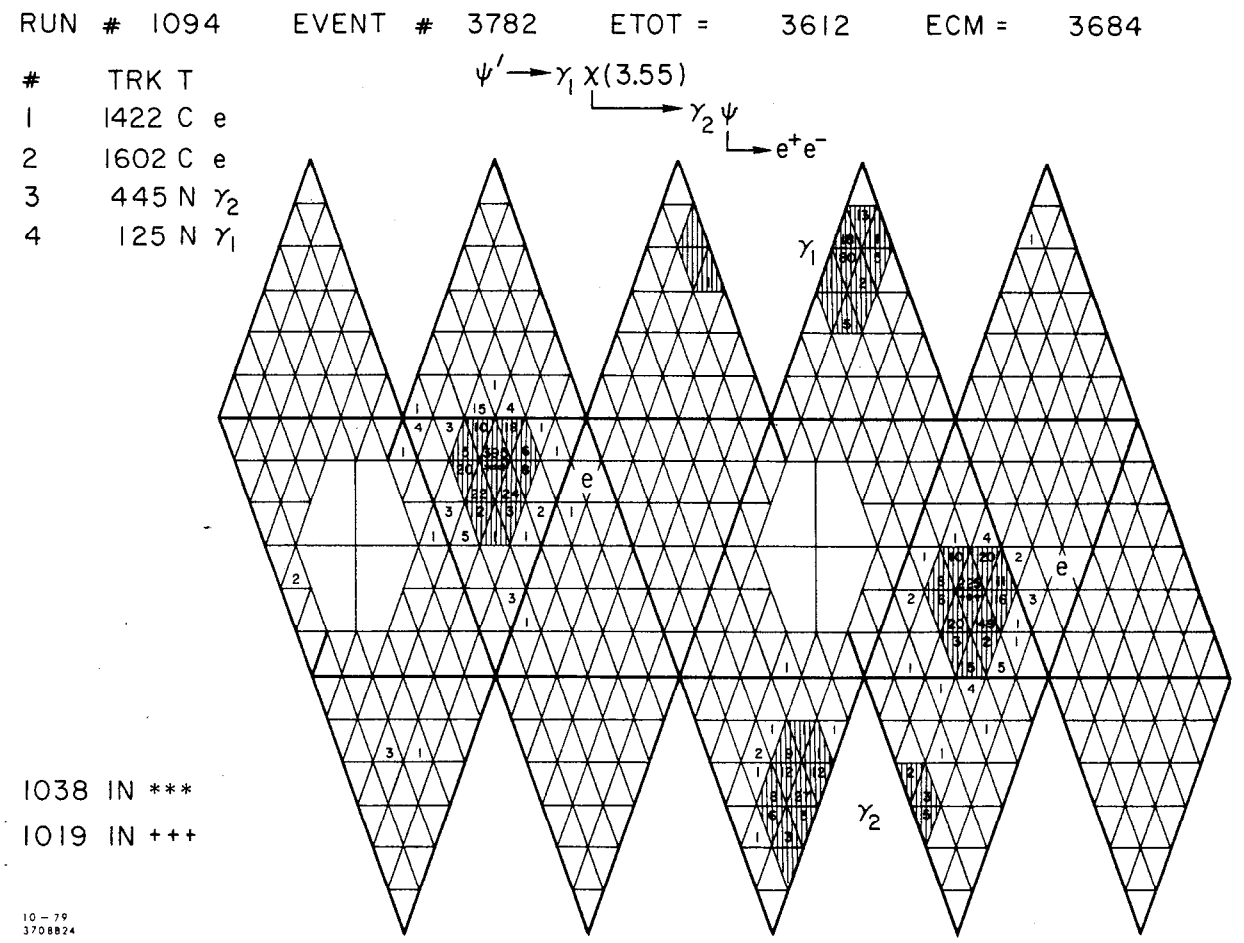

Fig. 17. A typical event of process (12). The cross lined regions indicate the sum of module energies used to estimate particle energies, and photon angles.

Table V

Crystal Ball Cascade Preliminary Results,
BrC ≡ Br($\psi' \to \gamma\chi$) · Br($\chi \to \gamma J/\psi$)

$\chi(3510 \pm 4)$: 1027 events

BrC = 2.1% ± 0.07% (statistical)
± 0.21% (# ψ')
± 0.30% ($J/\psi \to \ell^+\ell^-$)
± 0.21% (acceptance)

$\chi(3555 \pm 4)$: 531 events

BrC = 1.13% ± 0.05% (statistical)
± 0.11% (# ψ')
± 0.16% ($J/\psi \to \ell^+\ell^-$)
± 0.15% (acceptance)

$\chi(3410 \pm 6)$:† 29 events, 13.0 estimated $\pi^o\pi^o$ background,

BrC < 0.05% (90% C.L.)

$\chi(3455)$: 23 events, 9 estimated $\pi^o\pi^o$ background,

BrC < 0.045% (90% C.L.)

$\chi(3591)$: 21 events

BrC < 0.06% (90% C.L.)

No other states yet seen.
† Mass obtained from ψ' inclusive photon spectrum.

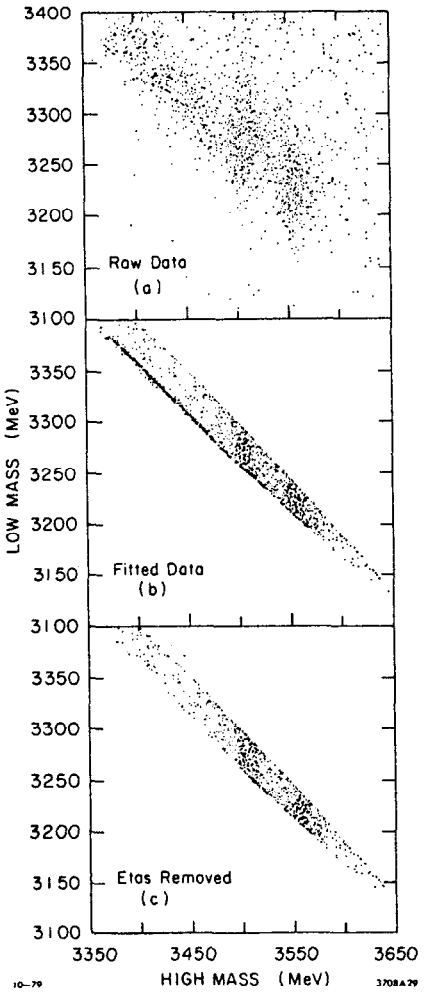

Fig. 18. Low mass vs. high mass scatter plots at various stages of analysis. (a) Raw data resulting from steps 1-5 of Table IV. Observed photon energies are used to calculate the plotted masses. (b) The data of (a) after kinematic fitting, 3C for $\gamma\gamma\mu^+\mu^-$, and 5C for $\gamma\gamma e^+e^-$ final states. (c) The data of (b) after η's are removed (see Fig. 19).

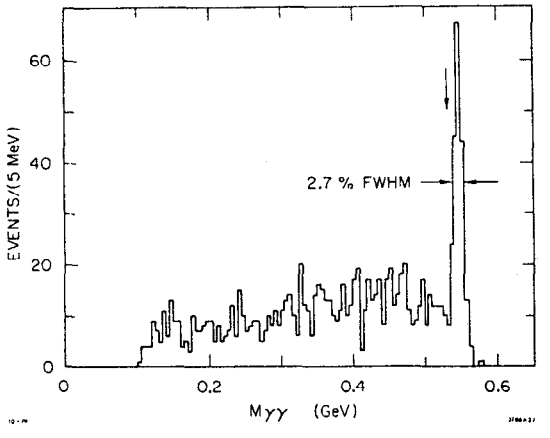

Fig. 19. $M_{\gamma\gamma}$ distribution for all fitted events of process (12) (see Fig. 18(b)). η's are removed in this analysis by a $M_{\gamma\gamma}$ cut at 530 MeV (vertical arrow in figure).

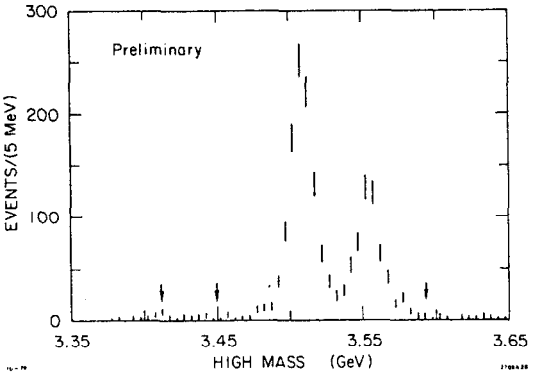

Fig. 20. The high mass projection of the scatter plot of Fig. 18(c). No signal is evident except $\chi(3555)$ and $\chi(3510)$. The vertical arrows indicate the positions of the states expected at 3415 MeV, 3455 MeV and 3591 Mev.

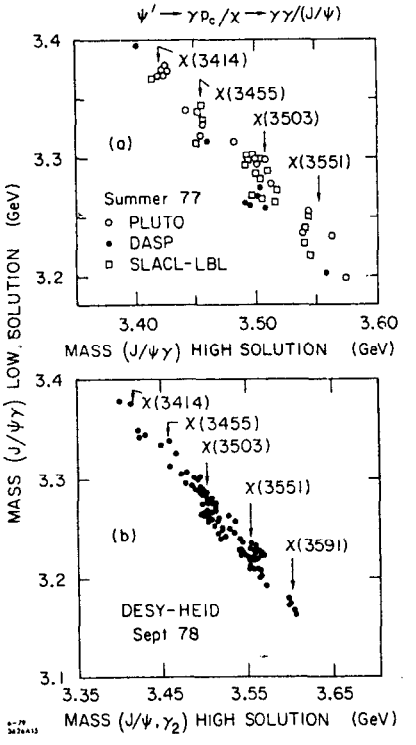

Fig. 21. A summary of the results of previous measurements of process (12). The results are shown as a scatter plot of low mass vs. high mass as was Fig. 18(c).

Table VI

Previous Results for $Br(J^P) \equiv B(\psi' \to \gamma\chi^{JP}) \cdot B(\chi^{JP} \to \gamma\, J/\psi)$

(SPIN Assignment are Educated Guesses)

Experiment	M_χ (1^+)	$Br(1^+)\%$	M_χ (2^+)	$Br(2^+)\%$	M_χ (0^+)	$Br(0^+)\%$	M_χ $(0^-)^\dagger$	$Br(0^-)\%$
DASP[26]	3508 ± 4	1.7 ± 0.4	3552 ± 6	1.4 ± 0.4	3413 ± 5^h	0.3 ± 0.2	--	< 0.4
Mark I[16]	3503 ± 4	2.4 ± 0.8	3551 ± 4	1.0 ± 0.6	3414 ± 3^h	0.2 ± 0.2	3454 ± 7	0.8 ± 0.4
Pluto[26]	seen	$1.2^{+1.0}_{-0.6}$	seen	$0.9^{+1.0}_{-0.5}$	seen	$0.7^{+0.8}_{-0.5}$	seen	$1.2^{+0.9}_{-0.6}$
DESY-Heid[27]	3505 ± 3	2.5 ± 0.4	3551 ± 4	1.0 ± 0.2	3420 ± 10	0.14 ± 0.09	--	$< 0.25^*$

h Mass determined from hadronic decays.
* New state reported, $\chi(3591 \pm 7)$, $Br(0^-) = (0.18 \pm 0.06)\%$.
† Mark II preliminary result:[28] $Br(3455) < 0.12\%$ (90% C.L.).

(c) The Cascade Angular Correlations and the Spin of the χ's

As described in Ref. 29, a determination of the spin of the X's and the multipolarity of the photon transitions in the cascade can be made by analyzing the angular correlations among the particles of the cascade. In Fig. 22 is shown a definition of the kinematics of the cascade process. With $\vec{\gamma}'$ the three vector of the first photon and $\vec{\gamma}$ the three vector of final photon of the cascade, we define

In Lab Frame: $\cos\theta' = \hat{z} \cdot \vec{\gamma}'/|\vec{\gamma}'|$,

$$\tan\phi' = \frac{\hat{z} \cdot (\vec{\gamma}' \times \vec{\gamma})}{\hat{z} \cdot \left[(\vec{\gamma}' \times \vec{\gamma}) \times \left(\frac{\vec{\gamma}'}{|\vec{\gamma}'|}\right)\right]}$$

($\hat{z}$ is direction of e^+ beam)

In χ Frame: $$\cos\theta_{\gamma\gamma} = \frac{\vec{\gamma}' \cdot \vec{\gamma}}{|\vec{\gamma}'||\vec{\gamma}|} \qquad (13)$$

In J/ψ Frame: $$\cos\theta = \frac{\vec{\ell}^{\pm} \cdot \vec{\gamma}}{|\vec{\gamma}||\vec{\ell}^{\pm}|}$$

$$\tan\phi = \frac{\vec{\ell}^{\pm} \cdot (\vec{\gamma}' \times \vec{\gamma})}{\vec{\ell}^{\pm} \cdot \left[(\vec{\gamma}' \times \vec{\gamma}) \times (\vec{\gamma}/|\vec{\gamma}|)\right]}$$

where all 3-vectors are evaluated in the frame specified. The angular correlation function which results is a function of all five angles defined in (13).

An initial attempt has been made to use the correlations, plus other information to obtain the spins of the χ states.[16] Tentative assignment of 2^+ to χ(3555) and 1^+ to χ(3510) has been made[17] based on a very limited amount of data. The Crystal Ball results presented here represent greater than a factor of ten more data than contained in the previous Mark I analysis. Thus, even though our spin analysis is still in its very preliminary stages, I will present some initial results on the χ spin determinations from our data. Ideally, a full angular correlation analysis should be made on the events to extract the greatest possible amount of information. This analysis is still in progress, and so here I will present only one dimensional (single angle) distributions to compare with the previous spin assignments, assuming E 1 dominance for the multipolarity of the γ transitions.

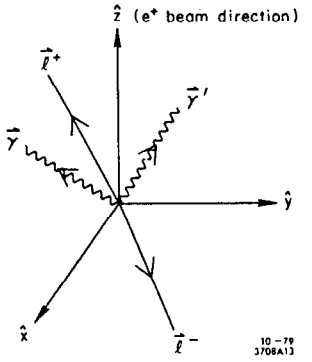

Fig. 22. The kinematics of process (12), definition of coordinate system.

Figure 23 shows the angular distributions from χ(3555). The data is shown with statistical errors only. A Monte Carlo result assuming spin 2 for this χ state and E 1 dominance for the multipolarity of the photon emissions is also shown. Reasonable agreement is seen between data and Monte Carlo. This is also true in Fig. 24 which presents χ(3510) angular distributions and spin 1,E 1 dominated Monte Carlo. Thus at present we find no conflict with previous spin, multipolarity assignments to χ(3555) and X(3510) cascades. However, our present analysis does not exclude other spin assignments and other multipolarities. We expect that the full correlation analysis will allow a more definite determination.

(d) The Hadronic Width of χ(3410) and QCD

The small upper limit to the χ(3410) cascade branching fraction is a surprising result given current theoretical models of the 0^+ decay process. One such model, the lowest order QCD estimation of the hadronic width of the χ states is represented in Fig. 25. Two gluons are exchanged in this model for 0^+, 2^+ hadronic decays, while 3 gluons are exchanged for 1^+ decay. A detailed calculation of these processes has been made[30] and results in predicted ratios for the hadronic widths of the χ states. The theory predicts for 1^- gluons,

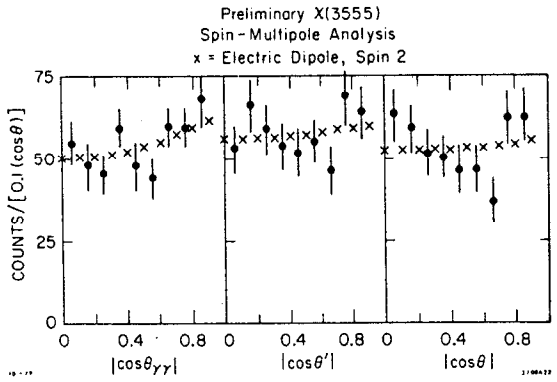

Fig. 23. Angular distributions for photons in process (12) for X(3555); see text for definition of angles. The points with error bars are data, x's are Monte Carlo.

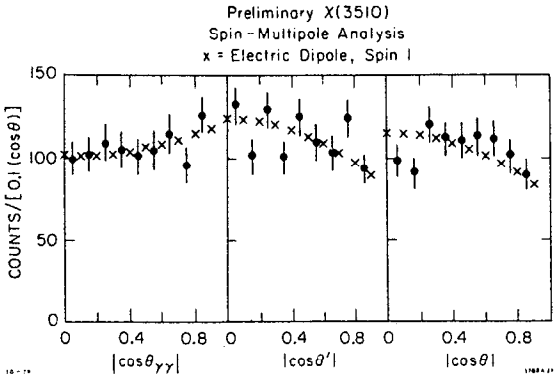

Fig. 24. Angular distributions for photons in process (12) for X(3510); see text for definition of angles. The points with error bars are data, x's are Monte Carlo.

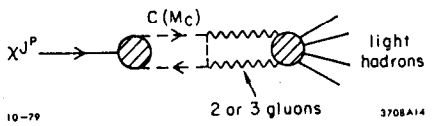

Fig. 25. Schematic representation of lowest order QCD calculation of χ^{J^P} decay into hadrons. C is charmed quark with mass Mc. Two gluons contribute to 0^+ and 2^+ decay, three gluons to 1^+ decay.

$$\Gamma(0^+\to h):\Gamma(1^+\to h):\Gamma(2^+\to h) = 1:\frac{4\alpha_s}{9\pi}\ln\left(\frac{4M_c^2}{4M_c^2-(3510)^2}\right):\frac{4}{15}\,. \tag{14}$$

Many theorists believe the 0^+, 2^+ ratio to be very reliable since both involve two gluon exchange, and so only a "clebsch" is involved in their ratio. I will concentrate here on this ratio since the ratios to the 1^+ are thought to be less reliable.

The results of the last section indicate consistency of the data with the canonical J^P, multipolarity assignments of the charmonium model, and so these are assumed in the following. Using our presently measured upper limit on the $0^+(3410)$ cascade, and the analysis of Ref. 17 as applied to Crystal Ball data, I find (see also the talk of C. Quigg at this conference),

$$\frac{\Gamma(2^+\to h)}{\Gamma(0^+\to h)} \lesssim 0.07\,. \tag{15}$$

The theory expects this ratio to be 0.27. Thus, qualitatively taking into account our experimental errors I find a factor of two to four disagreement with the theory. Qualitatively, the 0^+ seems too broad as compared to the 2^+. The resolution of this disagreement may lie in consideration of higher order QCD contributions to the hadronic widths. This point is discussed briefly by J. Ellis in his report to this Conference.

(e) Inclusive Photon Studies at the ψ'

We have presently analyzed essentially all ψ' data for the process,

$$\psi' \to \gamma + \text{anything} \tag{16}$$

and these results will be presented here.

The J/ψ data has not yet been fully analyzed for the process,

$$J/\psi \to \gamma + \text{anything} \tag{17}$$

and so I will not present any results on the J/ψ inclusive at this Conference.

The cuts used to select photons appearing in the inclusive spectrum of Fig. 26 are shown in Table VII.

Table VII

Cuts Used to Generate Inclusive γ Spectra

(1)	Hadronic events are selected in a manner similar to that shown in Table II.
(2)	$\lvert\cos\theta_i\rvert < 0.85$, for all particles, θ_i is the particle angle to the e^+ beam.
(3)	Charge particle-photon angular cut, $\cos\theta_{CG} < 0.85$.
(4)	Identified charged particles are removed.
(5)	π^o's are subtracted with a currently used algorithm which removes about 0.5 π^o per event.
(6)	For the remaining photons, 50 MeV < E_γ < 1000 MeV.

Note that the abcissa in Fig. 26 is $\ell n\, E_\gamma$. This is because our fractional energy resolution changes only by a factor of 2 over the range of E_γ shown. Steps (3) and (5) of Table VII introduce inefficiencies for the remaining photons which vary smoothly as a function of E_γ. We need a Monte Carlo simulation of the hadronic production process in order to estimate these inefficiencies accurately. This Monte Carlo is not yet available and so only very approximate estimates of absolute branching fractions can be made.

The purpose of my presentation is not to give absolute branching fractions on the known χ states, but to present evidence for the existence of a new state U(2.98) seen under the arrow in Fig. 26. The well-

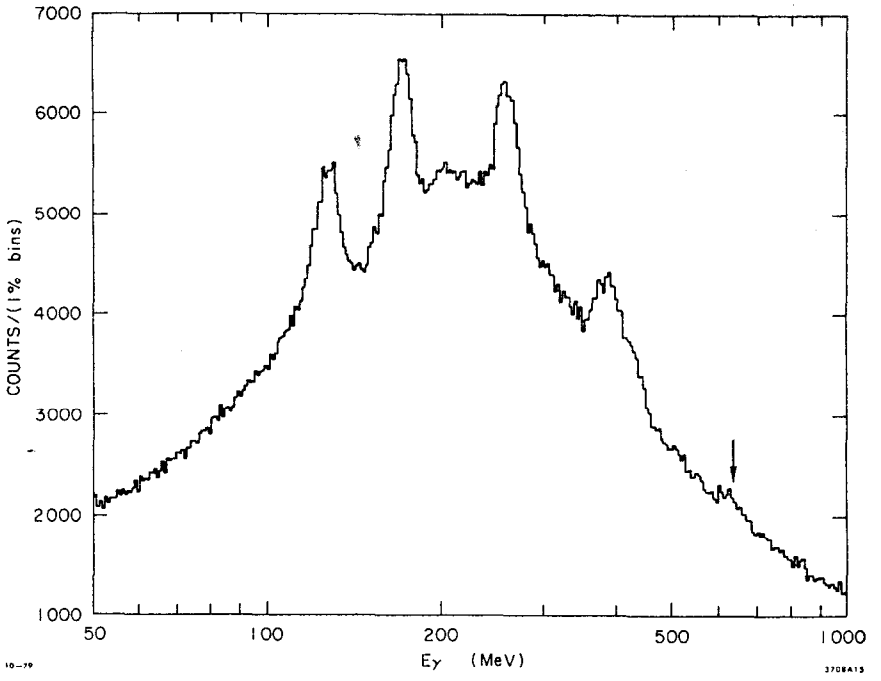

Fig. 26. Preliminary inclusive photon spectrum generated from 800K ψ' events. The cuts which are used to produce this spectrum are given in Table VII. The well-established states $\chi(3555)$, $\chi(3510)$ and $\chi(3410)$ are clearly evident starting on the left. The next bump to the right is the second cascade photons from $\chi(3555)$ and $\chi(3510)$. The last little bump (under the arrow) is a new state U(2.98 ± 0.02).

established χ states, $\chi(3410)$, $\chi(3510)$, and $\chi(3555)$ are evident in the figure. Also clearly seen, but not relatively so large is a bump at $E_\gamma = 0.64 \pm 0.02$ GeV corresponding to a mass of, $M_U = 2.98 \pm 0.02$ GeV. This result is more clearly seen in Fig. 27 where a blowup of the region of the new state is shown. Figure 27(a) shows the data, fitted with a function. This function is the sum of a Gaussian of arbitrary amplitude and position and relative width, $\sigma_o = 0.038$, fixed at about our resolution, plus a quadratic background. σ_o was obtained by first allowing a variable σ in the fit. The resulting σ_o was then fixed for subsequent fits. The background was fit both separately, and also simultaneously with the variable Gaussian parameters. Both techniques yielded state parameters equal within errors. In both cases the statistical significance of the effect was over 5 standard deviations. A particular fit yielded,

$$E_\gamma^U = 634 \pm 20 \text{ MeV}$$

$$\text{Estimated Yield U} = 1624 \pm 252 \text{ counts}$$

Figures 27(a) and (b) show the results of this fit. In Fig. 27(b) the fitted background has been subtracted yielding an obvious indication of a state.

We call this state U since its nature is presently unknown.[31] Using essentially educated guesses of our photon efficiency in the region of 600 MeV I estimate,

$$Br(\psi' \to \gamma U) = 0.2\% \text{ to } 0.5\%$$

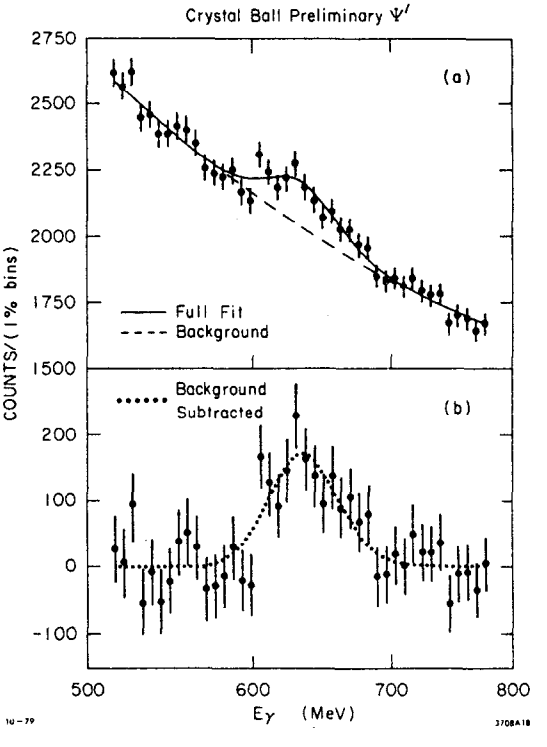

Fig. 27. A blowup of the ψ' inclusive photon spectrum in the region of the U(2.98 ± 0.02). (a) shows the fit to the data described in the text. Full fit and background from the fit are shown. (b) shows the data with background (as estimated from the fit) subtracted. A greater than 5σ effect is seen at E_γ = (634 ± 20) MeV.

Summary

A number of major conclusions can be drawn from the results presented in this report:

(1) The richness of continuum physics at SPEAR energies is yet to be fully revealed.

(2) The X(2820) and $\chi(3455)$ 0^{-+} candidates are not seen by the Crystal Ball.

(3) A new state has been discovered, U(2.98 ± 0.02 GeV), by examining our inclusive photon spectrum at the ψ'; we are in the process of examining our J/ψ inclusive photon spectrum for indications of the U there.

(4) The "old fashioned" non-relativistic charmonium model may not be so bad after all.

References

1. The members of the Crystal Ball Collaboration are: California Institute of Technology, Physics Department; R. Partridge, C. Peck and F. Porter. Harvard University, Physics Department; W. Kollman, M. Richardson, K. Strauch and K. Wacker. Princeton University, Physics Department; D. Aschman, T. Burnett, M. Cavalli-Sforza, D. Coyne and H. Sadrozinski. Stanford Linear Accelerator Center; E. Bloom, F. Bulos, R. Chestnut, J. Gaiser, G. Godfrey, C. Kiesling and M. Oreglia. Stanford University, Physics Department and High Energy Physics Laboratory; R. Hofstader, I. Kirkbride, H. Kolanoski, A. Liberman, J. O'Reilly and J. Tompkins.
2. E. D. Bloom, XIVth Recontre de Moriond, Les Arcs, France, March 11-23, 1979, Proceedings edited by Tran Thanh Van, Vol. 2.
3. B. H. Wiik and G. Wolf, "A Review of e^+e^- Interactions," DESY preprint 78/23, May 1978.
4. E. Higler et al., Phys. Rev. D15, 1809 (1977).
5. M. E. Law et al., Lett. Nuovo Cimento 11, 5 (1974).
6. G. Hanson et al., Lett. Nuovo Cimento 7, 587 (1973).
7. V. E. Balakin et al., Phys. Lett. 34B, 99 (1971).
8. C. Bacci et al., Lett. Nuovo Cimento 2, 73 (1971).
9. G. Feldman, Rappoteur talk in the Proceedings of the XIX International Conference on High Energy Physics, Tokyo, Japan, August 23-30, 1978; also, SLAC-PUB-2224 (1978).
10. J. Kirkby, presentation at this conference.
11. R. Schwitters, in Proceedings of the 1975 International Symposium on Lepton Photon Interactions at High Energies, edited by W. T. Kirk (Stanford Linear Accelerator Center, Stanford University, Stanford, California, 1976), p. 353.
12. G. Goldhaber et al., Phys. Rev. Lett. 37 255 (1976); I. Peruzzi et al., Phys. Rev. Lett. 37, 569 (1976).
13. G. Feldman, in Proceedings of 5th International Conference on Meson Spectroscopy, Boston, Mass., April 29-30, 1977, edited by E. Von Goeler and R. Weinstein, Northeastern University, press.
14. S. J. Brodsky et al., Phys. Lett. 73B, 203 (1978).
15. From the talk of G. Flügge, in Proceedings of the XIX International Conference on High Energy Physics, Tokyo, Japan, August 23-30, 1978.
16. W. M. Tanenbaum et al., Phys. Rev. D17, 1731 (1978).
17. M. S. Chanowitz and F. J. Gilman, Phys. Lett. 63B, 178 (1976).
18. Braunschweig et al., Phys. Lett. 67B, 243 & 249 (1977); also see Ref. 3.
19. W. D. Apel et al., Phys. Lett. 72B, 500 (1978).
20. J. S. Whitaker et al., Phys. Rev. Lett. 37, 1596 (1976).
21. C. J. Biddick et al., Phys. Rev. Lett. 38, 1324 (1977).
22. For a comprehensive review of the charmonium model see: T. Appelquist et al., Ann. Rev. Nucl. Part. Sci. 28 (1978); also, SLAC-PUB-2100 (1978).
23. K. Gottfried, in the Proceedings of 1977 International Symposium on Lepton and Photon Interactions at High Energies, DESY, edited by F. Gutbrod (1978).
24. V. Novikov et al., Phys. Lett. 67B, 409 (1977); N. A. Shifman et al., Phys. Lett. 77B, 80 (1978). These papers indicate strongly the necessity in the charmonium model of an η_c with mass close to 3.0 GeV.
25. C. Keisling, in the Proceedings of the 1979 EPS High Energy Physics Conference, Geneva, Switzerland, June 27-July 4, 1979.
26. H. Spitzer, in the Proceedings of the Kyoto Summer Institute for Particle Physics, Kyoto University, Japan, September 1-5, 1978; also, DESY 78/56 (1978).
27. W. Bartel et al., Phys. Lett. 79B, 492 (1978).
28. Mark II preliminary results also do not confirm those of Ref. 16. See: D. L. Scharre, in Proceedings of the XIVth Recontre de Moriond, Les Arcs, France, March 11-23, 1979, Proceedings edited by Tran Thanh Van, Vol. 2.
29. G. Karl et al., Phys. Rev. D13, 1203 (1976).
30. R. Barbieri et al., Phys. Lett. 60B, 183 (1976); R. Barbieri et al., Phys. Lett. 61B, 465 (1976); see also Ref. 22.
31. H. Harari, First suggested the use of "U for unknown" at the time of the discovery of what is now called τ. For additional discussion of the U(2.98) see his talk at this conference.